



LAWRENCE  
LIVERMORE  
NATIONAL  
LABORATORY

# Systematic Source Determination and X-ray Radiography Detection of Nonuniformities on High-Density Carbon Ablators

M. G. DeVincenzi, A. Nikroo, B. Kozioziemski , J.  
Hackbarth, T. Braun , I. Chavez, E. Piceno

October 28, 2022

Fusion Science and Technology

## **Disclaimer**

---

This document was prepared as an account of work sponsored by an agency of the United States government. Neither the United States government nor Lawrence Livermore National Security, LLC, nor any of their employees makes any warranty, expressed or implied, or assumes any legal liability or responsibility for the accuracy, completeness, or usefulness of any information, apparatus, product, or process disclosed, or represents that its use would not infringe privately owned rights. Reference herein to any specific commercial product, process, or service by trade name, trademark, manufacturer, or otherwise does not necessarily constitute or imply its endorsement, recommendation, or favoring by the United States government or Lawrence Livermore National Security, LLC. The views and opinions of authors expressed herein do not necessarily state or reflect those of the United States government or Lawrence Livermore National Security, LLC, and shall not be used for advertising or product endorsement purposes.

# **Systematic Source Determination and X-ray Radiography Detection of Non-Uniformities on High Density Carbon Ablators**

M. G. DeVincenzi,<sup>1\*</sup> A. Nikroo,<sup>1</sup> B. Kozioziemski,<sup>1</sup> J. Hackbarth,<sup>1</sup>  
T. Braun,<sup>1</sup> I. Chavez,<sup>1</sup> E. Piceno<sup>2</sup>

<sup>1</sup>*Lawrence Livermore National Laboratory, Livermore, California*

<sup>2</sup>*General Atomics, San Diego, California*

\*E-mail: devincenzi3@llnl.gov

# Systematic Source Determination and X-ray Radiography Detection of Non-Uniformities on High Density Carbon Ablators

M. G. DeVincenzi,<sup>1\*</sup> A. Nikroo,<sup>1</sup> B. Kozioziemski,<sup>1</sup> J. Hackbarth,<sup>1</sup> T. Braun,<sup>1</sup> I. Chavez,<sup>1</sup>  
E. Piceno<sup>2</sup>

<sup>1</sup>*Lawrence Livermore National Laboratory, Livermore, California*

<sup>2</sup>General Atomics, San Diego, California

Recent deuterium-tritium (DT) layered implosion experiments at the National Ignition Facility have achieved a burning plasma and >1MJ neutron yield. A series of repeat experiments have shown that the degree of performance is very likely dependent on capsule quality including the quantity of what are collectively termed “high Z particles.” These “particles” are detected on a custom-built radiography system known as the Sagometer during the final target qualification process. The term “particles” is misleading as the source of these non-uniformities in capsule images is uncertain; the term detection will be used instead. An increased number of DT targets have been rejected at the final stages of production due to Sagometer detections. Late detections are deleterious in terms of loss of production parts, effort, and overall operating efficiency. In response, we undertook an effort to determine the origin of these detections and to ultimately mitigate target losses caused by them. Through careful testing and analysis, we have determined neither insufficient production cleanliness nor hohlraum shedding is responsible for the detections on the capsule. We determined that the detections are inherent to the capsule and made efforts to use the Zeiss Xradia to identify them earlier in the production process. While testing revealed the Xradia is not currently sufficient for identifying such “particles” using radiography images, we continue to look to other forms of metrology to down select the capsules early in the process.

Keywords: capsule; radiography; Sagometer; tomography; HDC

## I. INTRODUCTION

Recent Inertial Confinement Fusion (ICF) experiments at the National Ignition Facility (NIF) have achieved a burning plasma and >1MJ neutron yield by imploding a high-density carbon (HDC) capsule with internally layered deuterium-tritium (DT) ice.

A series of repeat experiments have shown that the degree of performance is very likely dependent on capsule quality including void and pit content of the capsules, but also the quantity of what are collectively termed “high Z particles.” Defects and high Z particles can result in ablator mixing into the hot spot, causing hydrodynamic instabilities and lower neutron yield.<sup>1,2</sup>

The “high Z particle” detection is performed just prior to target approval for use in the NIF experiment and is used to establish final cleanliness of the capsule. This inspection is typically performed on a custom-built radiography system known as the Sagometer. The term “high Z particle” is misleading as it assumes the feature in the image is in fact a particle composed of high Z material. Instead of “high Z particle”, the term “detection” will be widely used in this paper. The term is intentionally nondescript as to not assume a source or cause. A detection is one or more pixels of high contrast with respect to the surrounding pixels, in an area on the capsule in which we expect uniformity. In other words, a detection is a non-uniformity in the capsule image, which could be caused by a particle, a change in density in the shell, or any other unknown source. Due to an increased number of DT targets being rejected due to Sagometer detections, we have undertaken an effort to better understand the origin of these detections and to ultimately mitigate them, with the goal of saving valuable effort and time.

The effort began by examining depleted uranium (DU) hohlraum shedding, capsule handling cleanliness at Lawrence Livermore National Laboratory (LLNL), and capsule processing cleanliness at General Atomics (GA). We reviewed historical data and used simple statistics to investigate the DU hohlraums as a source of particulation. We then conducted surface and air particulation studies at both LLNL and GA to evaluate production cleanliness as another possible source of particulation. Finally, we

analysed the imaging configuration on the Sagometer and applied what we learned to settings on the Zeiss Xradia at GA in an effort to detect the “high Z particles” much earlier in the production process. We compared the settings by imaging capsules on both machines in the same orientation and processing the images with software for unbiased evaluation of particle detection ability.

## **II. POSSIBLE SOURCES OF SAGOMETER DETECTIONS**

HDC capsules are made in Germany by coating a silicon mandrel with HDC. The capsules are then shipped to GA in San Diego. GA drills a hole in the shell wall, leaches the mandrel out, and processes the capsule, which includes a metrology step to check for detections. The GA processing concludes with attaching a fill tube in the previously drilled hole. The capsule fill tube assembly (CFTA) is then shipped to LLNL in clean packaging where it undergoes LLNL processing before being installed into a target. Figure 1 depicts the simplified capsule lifecycle, from the moment it arrives at GA to the final metrology step at Target Fabrication’s (TFAB’s) Sagometer. Also depicted in Figure 1 is the presence of detections at Sagometer that did not present during GA’s Xradia defect check.

Fig. 1. Summary of HDC capsule lifecycle in terms of processing steps at GA and LLNL.<sup>3</sup>

There was an assumption that the capsules arrive at LLNL free of any and all possible Sagometer detections. Because of this, the focus was initially on the cleanliness of LLNL processing and handling of the capsule. At the early stages of the effort, depleted uranium (DU) hohlraum shedding and cleanliness were the main suspected causes of the Sagometer detections. Both sources were considered and analysed using statistical methods and careful testing. Figure 2 shows the cross section of a typical DT

target with a suspected source and various possible locations of “particles” shown as dots. Though the assumption that capsules arrived at LLNL detection free would suggest detections were on the surface of the capsule, we acknowledged the true location of the detections was unknown. It is important to note that Sagometer imaging does not have the spatial resolution to determine if the detection is on the exterior of the capsule, in the capsule wall, or on the interior of the capsule.

Fig. 2. Possible locations of particles causing Sagometer detections on a typical ICF target. Shown is the HDC capsule suspended by tents inside of a DU or gold hohlraum.<sup>3</sup>

### ***II.A. Depleted Uranium Hohlraum Shedding***

A target capsule is imaged on Sagometer through the laser entrance holes (LEHs) creating a 2D projection of the capsule and tent through the hohlraum openings at the top and bottom LEH, outlined in Figure 2 as light green rings. The capsule is suspended by two thin formvar films referred to as tents.<sup>4</sup> The tents are secured to the two hohlraum halves and apply pressure to the capsule, holding it in place. Although the tent only contacts the top/bottom of the capsule before lifting off, Sagometer is unable to distinguish whether a detection is on the lifted-off portion of the tent or the capsule itself.

Fig. 3. Projected areas of the capsule and tents as they are seen in Sagometer images. This view is looking through the top and bottom LEH at the capsule.<sup>3</sup>

For this reason, the focus is on the projected area of the entire capsule (A+B in Figure 3) and the projected area of the “tent only” region that is not covered by the capsule (C), although statistical analysis was conducted to compare all three areas. It is important to note that the projected area of the entire capsule is approximately equal to the projected area of the tent only region around the capsule. One theory is that over

time, the inside wall of the DU hohlraums begin to oxidize and delaminate,<sup>5</sup> shedding particles on the capsule and tents.

Fig. 4. Review of Sagometer detections on three different hohlraum types, and the location of the detections.<sup>3</sup>

A review of historical Sagometer data from 123 targets (Figure 4) revealed that the overwhelming majority of detections are located in the projected area of the capsule (A+B). For targets with gold lined DU hohlraums, close to 1% of detections across 72 targets were in the tent only area. For targets with liner-less DU hohlraums (or DU hohlraums without a gold lining on the interior surface), less than 14% of detections across 20 targets were in the tent only area. Considering the projected area of the capsule and the tent are about equal, one would expect the number of particles in each region to be equal as well. This is not the case with the 123 targets reviewed, therefore, it is statistically unlikely that a majority of detections identified at Sagometer are due to the DU hohlraums shedding onto the capsule.

### ***II.B. Cleanroom Cleanliness and Capsule Handling***

When the capsule arrives at LLNL, it has already been attached to a fill tube at GA, and therefore is considered a CFTA. The CFTA goes through 18 processing steps in the LLNL cleanroom before it arrives at Sagometer. To quantify the risk of particles being deposited on the capsule during LLNL CFTA processing, surface particulation monitoring was conducted for each process both through surface and airborne particle counting techniques.

To obtain a single measurement, data is collected for a week and then converted to units of particles accumulated per hour per capsule using historical data for the length of each process and the known capsule diameter. We collected this data for five months and used the worst-case measurement for particles per day in our calculations. The data

suggests that on average LLNL processing is responsible for depositing less than one particle on the capsule per target build; this is far less than the 5-20 particles we were detecting at Sagometer.

Fig. 5. Worst-case total particles accumulated on the capsule during a standard DT target build at LLNL.<sup>6</sup>

### *II.B.1. Wafer Tests*

To assess general cleanliness of surfaces in the lab, as well as the cleanliness of specific processes, four-inch silicon wafers are placed at each station outlined in Figure 5. The wafers are first cleaned using a piranha etch to ensure they are free of contamination and particles. A Zeiss Axio Imager Z2 Vario microscope running a particle detection routine is used to take a baseline measurement of the particles on the surface of the wafer. Then, the wafers are placed at stations as close to the work area as possible and left undisturbed for a week in the cleanroom to collect particles that fall from the air or that are generated during a process. Finally, the wafers are placed back on the Zeiss microscope for a second particle count measurement. The baseline is subtracted from this measurement, and the net particle count is used to calculate particles per unit area, per hour. The Zeiss program inspects the same 2" X 2" square at the centre of the wafer and is programmed to detect particles greater than five microns in diameter. Using wafer test data from the worst week, we calculated a total contribution of 0.7 particles per capsule during a standard DT target build.

### *II.B.2. Air Monitoring*

A Lighthouse Handheld 5016 particle counter is used in the cleanroom to quantify the particles in the air that do not land on surfaces (or the wafers), but still have the potential to land on the capsule. This particle counter samples 0.1 cubic feet of air

every minute and is capable of detecting airborne particles from 0.5 microns to 25 microns in diameter. Similar to the wafers, the particle counter is placed at each station of interest close to the work being performed. The calculated particle contribution from the cleanroom air is 0.00 particles per capsule during a standard DT target build, which is expected due to the redundant air filtration in the cleanroom.

### ***II.C. Capsule as Received from GA***

With DU hohlraum shedding and cleanroom cleanliness both showing minor contributions to Sagometer detections, the next step was to test the assumption that capsules coming from GA should have no detections.

Around the time of this testing, a beryllium capsule built into a target with a gold hohlraum showed 18 detections at Sagometer, and its backup target with the same configuration showed eight detections. For both of these targets, all detections were in the projected area of the capsule, which is expected for gold hohlraums (see Figure 4). At worst, LLNL handling can add a single particle to the capsule but cannot account for 8 or 18 particles. Considering all detections were in the projected area of the capsule, gold hohlraums statistically do not shed, and the cleanroom has exceptional cleanliness, a strong case was made that detections are on the capsule prior to arrival at LLNL.

To test the assumption that capsules came clean of detections from GA, we pulled a capsule off a CFTA without any contact with tooling or personnel and imaged the capsule on Sagometer. The CFTA remained sealed in a double bag and had not been handled at all at LLNL prior to detachment. It was taken to the “cleanest” part of the cleanroom (according to cleanliness data) where the CFTA was removed from the GA double bag packaging and the capsule was pulled off the fill tube using a clean tacky film. The capsule on tacky film was immediately placed in Sagometer, and the images

showed more than twelve detections. This disproved the assumption that the capsules are free of detections when they arrive at LLNL.

#### ***II.D. Capsule Batch and Detections***

The beryllium capsule test proved detections are present on the capsule when they arrive from GA, so they could be coming from GA processing and handling. GA and LLNL collaborated to assess the GA cleanroom cleanliness with identical wafer and airborne particle counter monitoring. Their results also showed that GA processing is responsible for depositing less than one particle on a capsule per build. This would suggest that the detections could be inherent to the capsules themselves and are not added in processing steps.

To explore this further we analysed Sagometer detections by capsule, grouped by the batch they were made in (Figure 6). Although the range of detections per capsule can vary greatly within each batch, there is a strong correlation present. If a capsule from a single batch shows a high number of detections, it is very likely that other capsules from that batch will have a high number of detections as well.

Fig. 6. Capsule detections by manufacturing batch.<sup>3</sup>

### **III. IDENTIFYING DETECTIONS EARLY IN PROCESSING**

Based on the data collected and analysed, it seemed evident that detections were inherent to the capsule, and not identified in GA's metrology steps but caught on Sagometer. The goal was then to identify capsule detections at the beginning of the process before the fill tube is attached at GA (see Figure 1). GA uses an off the shelf x-ray imaging system from Zeiss, the Xradia Versa 510, while LLNL uses the Sagometer, a system designed and constructed internally.

TABLE I. Specifications for x-ray imaging systems used in Target Fabrication.

### ***III.A. Current Particle Detection Imaging***

GA characterizes capsule quality with the Xradia in three ways, two radiography images and a tomography scan. The two radiography images taken on Xradia are most similar to the Sagometer images; both image sets are for “particle detection.” The tomography scans create a 3D reconstruction of the capsule, but the scans take hours to complete, making them less practical for quick down selection of capsules in production. The Sagometer images take about 45 minutes to collect, and the Xradia 2D images are similarly within an hour. The two images taken on Xradia are a 4X radiography image and a 20X mosaic radiography image in which multiple images are taken in a mosaic pattern and then stitched together by the Xradia software.

Fig. 7. Sagometer detections on an HDC capsule.

Initially, the detections we were seeing on Sagometer were thought to be “high Z” material because they showed up as dark detections in the images (as in Figure 7). It turns out that low Z particles can be imaged on both Sagometer and Xradia. We confirmed this by applying 10-30  $\mu\text{m}$  diameter polyimide and nylon particles to a capsule and imaging the capsule on both systems. We found that these low-density particles not only appeared in the radiography images, but appeared as dark spots on the images. This means that the dark detections on Sagometer could be composed of a wide range of materials, not just the high Z material that was initially assumed.

Fig. 8. Sagometer (a) and Xradia (b) radiographs of low Z particles (circled in red) on the same capsule.

The same particle group is shown in both images in Figure 8, and yet the particles appear to have more contrast in the Sagometer image than in the Xradia image. This difference in contrast is consistent for other images we looked at while comparing Xradia particle detection to Sagometer, and could be a reason the detections were only identified on Sagometer.

### ***III.B. Differences in Particle Detection Imaging***

This discrepancy in the images is in part due to the Sagometer system which was originally designed to take advantage of phase-contrast enhancement for the imaging, allowing us to see much lower Z material than traditional absorption-dominated imaging.<sup>7</sup> Phase-contrast enhanced x-ray imaging utilizes the minor refraction and diffraction of x-rays at abrupt changes in the density profile of features in the imaging field of view.<sup>8</sup> Using five different capsules, we compared images taken on Sagometer to images on Xradia and found that with GA's typical particle detection settings, fewer detections appeared on the Xradia images than did on the Sagometer images for the same shell.

There are several factors in the imaging system which influence the ability to detect features. These include the effective resolution in the object plane due to both x-ray source size and detector resolution, number of photons collected per resolution element, and the contrast enhancement due to the ability to resolve phase-contrast enhancement.<sup>9</sup> However, since the Xradia and Sagometer use different detectors and different x-ray sources, it was not possible to directly match the Xradia with the Sagometer operating conditions. Instead, we attempted to make the two systems equal in terms of signal-to-noise so we could use Xradia in place of Sagometer at GA.

#### ***III.B.1. Phase-Contrast Enhancement***

First, we want to match the object-plane resolution of the two systems. The Sagometer has larger pixels, 20 microns compared to 3.37 microns at the Xradia scintillator. Also, the x-ray spot size is approximately five microns FWHM compared to 2.5-3 microns for the Xradia. Next, difference in the geometry can also change the amount of phase-contrast enhancement. Finally, the total number of collected photons will determine the shot-noise dominated signal-to-noise ratio of the measurement. This

depends on both source and detector characteristics, as well as the geometry, which is represented in Figure 9.

Fig. 9. X-ray imaging geometry for capsule radiography.

The system geometry, the source-to-object distance ( $SO$ ), and the object-to-detector distance ( $OD$ ), determine the resolution and phase-contrast enhancement. The geometry is also easy for us to manipulate on Xradia, within the limits of the system, so it was a focus in this effort. First and foremost, the  $SO$  and  $OD$  directly affect the geometric magnification,  $M_g$ .

$$M_g = 1 + \frac{OD}{SO} \quad (1)$$

The geometric magnification needs to be set to produce similar effective pixel sizes in the object plane.  $M_g$  needs to be larger for the Sagometer than the Xradia due to the difference in detector pixel sizes. Next, the x-ray spot size at FWHM,  $a$ , will result in a penumbral blur at the detector that depends on  $M_g$  as shown in Equation (2).

$$R_{PB} = a \frac{M_g^{-1}}{M_g} \quad (2)$$

The penumbral blur decreases as  $M_g$  is made smaller; however this must be balanced by the detector resolution, which favours larger  $M_g$ . Finally, for a cone-beam geometry, the relative amount of phase-contrast enhancement in the image is expressed as  $Z_{PW}$ .

$$\begin{aligned} Z_{PW} &= \frac{(OD)(SO)}{OD + SO} \\ &= \frac{OD}{M_g} \\ &= SO \frac{M_g^{-1}}{M_g} \end{aligned} \quad (3)$$

We can use these scaling equations to make the expected contrast and spatial resolution similar between the two systems. This leads to a difference in distances between source

and detector, which reduces the number of photons arriving per pixel as  $1/(OD+SO)^2$ .

The exposure time can be increased to compensate for fewer photons as the total distances are increased.

TABLE II. Xradia and Sagometer imaging settings tested for particle detection.

We tried several different configurations, imaging settings, and post processing contrast enhancement of images of the same capsule in the same orientation. To compare the detection ability of each system, we used a well-tested particle detection code coupled with manual inspection to count detections in images of the same capsule.. In some cases, the code failed to identify a detection in an Xradia image while manual inspection found it; in other cases, the data in Sagometer images was simply missing from the corresponding Xradia image. We looked at grayscale values of pixels, and if the value (or signal) was not high enough to differentiate from the noise in the area, then the signal was simply not identifiable in that image. Figure 10a shows one such example where the features of interest, circled in Figure 10b (Sagometer image), were not present in Figure 10a (the Xradia image).

Fig. 10. Xradia image (a) and Sagometer image (b) of the same capsule.

Detections identified by the software are circled in red.

### *III.B.2. Possible Causes of Imaging Discrepancies*

We found that even after optimizing imaging settings, Sagometer and Xradia did not match consistently. This is in part due to resolution from spot size and pixel size. The source and detector in Xradia are on software-controlled stages, so we were able to modify the  $SO$  and  $OD$  distances, but were limited by the space of the enclosure, which is smaller than Sagometer. We investigated changing the source to achieve a better spot size and reduce blur, but the other sources that Zeiss supports will not make a significant impact on the spot size.

There is also the issue of the Xradia detector, which is fundamentally different from the Sagometer detector. Sagometer uses a direct detection method in which the CCD itself detects the x-ray photons, which is ideal for this type of imaging.<sup>8</sup> Xradia, on the other hand, uses a scintillator within the objective to convert x-rays to visible light, which is then focused by the objective onto a visible light CCD. In addition, while the Xradia's detector is better at converting a wide range of x-ray photon energies, it tends to decrease contrast for lower density material in the image as the higher energy x-rays pass through features with little attenuation. The CCD in Sagometer, on the other hand, does not efficiently convert x-rays above 9 keV, which is advantageous for our imaging as it improves contrast for mid to low Z features. Changing the detector on Xradia is not a practical solution due to the complexity of the required hardware and software modifications.

Finally, increasing exposure time could help with the signal-to-noise ratio, but we found that at long exposures, random dark artifacts appear in the Xradia images. These artifacts detract from the actual features of interest in that they could mask or distort the actual features, making them extremely hard to detect. To eliminate these artifacts, we would either need to determine their root cause or remove them from images using software, without removing the detections of interest. Both options would require a significant amount of development and testing.

The two systems still differed even after trying to make their signal-to-noise as similar as possible. Part of the remaining discrepancy is there are differences in the detector response between the CCD (Sagometer) and scintillator (Xradia) which shifts the effective x-ray energy lower. This leads to increased contrast for the Sagometer.

#### **IV. CONCLUSION AND FUTURE EFFORTS**

An increase in radiography detections on ICF capsules first identified at final qualification have resulted in high rates of reject targets. These target rejections result in a substantial loss in production parts, effort, and operating efficiency. In response, a large effort was spurred to locate the source of these detections in the capsule lifecycle and to ultimately mitigate them.

The DU hohlraums used for these targets were the prime suspects for particulation, however, we have systematically made several determinations that contradict this hypothesis. We have shown that the Sagometer detections could be due not only to surface particles added in various steps of the production process but also contamination on the inner wall surface or imperfections within the shell wall, and in fact hardly associated with the DU hohlraums. We also determined that the Sagometer imaging configuration (phase contrast and detector response) is naturally sensitive not only to “high Z particles” but much lower Z particles as well. To catch such contamination in the upstream capsule fabrication process, we attempted to use the Zeiss Xradia at General Atomics in place of Sagometer, but discovered the system is not sufficient in its current configuration for this application. Finally, our future work will consist of exploring tomography data to determine if this step in the metrology process can be used to down-select capsules at an early stage.

Although tomography was not initially desirable due to the extensive time required for a single 3D scan, its potential relevance for adequate early particle detection became clear. This relevance was further supported by a test conducted during radiography imaging that used rotation between images to better understand the location of the detections. We monitored the location of detections as the capsule was rotated, and the trajectory showed most of the detections appeared to be in the wall or on the inner surface of the capsule. Tomography produces a 3D reconstruction of the capsule

in which we can look slice by slice to examine non-uniformities throughout the entire shell volume. Future work will focus on using tomography to down select capsules early in the process and further explore the origin and nature of the detections.

## **ACKNOWLEDGEMENT**

This work was performed under the auspices of the U.S. Department of Energy by Lawrence Livermore National Laboratory under Contract DE-AC52-07NA27344. LLNL-ABS-765894.

## REFERENCES

1. H. ABU-SHAWAREB, et al., “Lawson Criterion for Ignition Exceeded in an Inertial Fusion Experiment,” *Phys. Rev. Lett.*, **129**, 7, 75001 (2022).
2. A. L. KRITCHER, et al., “Design of inertial fusion implosions reaching the burning plasma regime,” *Nature Physics*, **18**, 251 (2022).
3. A. NIKROO, Target Fabrication and Physics, Lawrence Livermore National Laboratory, Source of particles seen in Sagometer images, Personal Communication (Mar. 2022).
4. M. STADERMAN, S. A. LETTS, S. BHANDARKAR, “Improvements to Formvar Tent Fabrication Using the Meniscus Coater,” *Fusion Science and Technology*, **59**, 1, 58 (2017).
5. K. J. M. BLOBAUM, et al., “Characterization of Blistering and Delamination in Depleted Uranium Hohlräume,” *Fusion Science and Technology*, **63**, 2, 232 (2013).
6. M. AGGLETON, et al., “Sources and Detection of Particles on Capsules,” presented at the 24<sup>th</sup> Target Fabrication Specialist Meeting, Virtual from Livermore, California, June 6-9, 2022.
7. T. E. GUREYEV, et al., “Some simple rules for contrast, signal-to-noise and resolution in in-line x-ray phase-contrast imaging,” *Optics Express*, **16**, 5, 3223 (2008).
8. B. J. KOZIOZIEMSKI, et al., “Quantitative characterization of inertial confinement fusion capsules using phase contrast enhanced x-ray imaging,” *Journal of Applied Physics*, **97**, 6, 063103 (005).
9. A. POGANY, D. GAO, S. W. WILKINS, “Contrast and resolution in imaging with a microfocus x-ray source,” *Review of Scientific Instruments*, **68**, 2774 (1997).

## TABLES

TABLE I. Specifications for X-ray imaging systems used in Target Fabrication

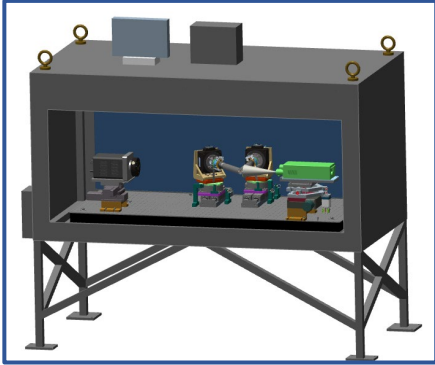

<b>System</b>		
	<b>LLNL Sagometer</b>	<b>Zeiss Xradia Versa 510</b>
<b>Detector</b>	X-ray CCD, PI-LCX-NTE/CCD-1340/1300-HER, 20 $\mu\text{m}$ pixels	Scintillator + visible light CCD camera, Zeiss proprietary, 3.37 $\mu\text{m}$ pixels
<b>Source</b>	Point Source, ThermoFisher PXS5-927EA-R-LV, 5 $\mu\text{m}$ spot	Point Source, Zeiss proprietary sealed transmission source, 3 $\mu\text{m}$ spot
<b>Source to object</b>	Static, 85 mm	Adjustable, 0-200 mm
<b>Object to detector</b>	Static, 536 mm	Adjustable, 0-330 mm
<b>Typical Radiograph Settings</b>	320s exposure time, 85mm/536mm (phase contrast enhancement)	30s exposure time, 15mm/25mm (contact radiography)
<b>Typical Tomography Settings</b>	No current capability	800 projections, 15s exposure per projection, 0-15mm/20-30mm (contact radiography)

TABLE II. Xradia and Sagometer imaging settings tested for particle detection.

Xradia Settings								
Setting	Potential, kV	Power	Filter	Exposure [s] X # Images	Detector Binning	SO	OD	Pixel size [ $\mu\text{m}$ ]
A	30	2	-	1200 X 1	2	-200	330	2.57
B	30	2	-	1800 X 1	2	-200	330	2.57
C	30	2	-	900 X 1	2	-200	330	2.57
D	60	2	-	1 X320	1	-89.5	150	1.27
E	60	2	-	320 X1	1	-89.5	150	1.27
F	60	2	-	640 X1	1	-89.5	150	1.27
G	50	4	-	30 X1	1	-15	25-30	1.27

H	50	4	-	15 X1	1	-15	25-30	1.27
I	30	2	20µm Zn	900 X1	2	-200	330	2.57
J	30	2	25µm Cu	900 X1	2	-200	330	2.57
K	30	2	50µm Cu	480 X1	2	-25	50	2.27
L	60	2	20µm Zn	900 X1	2	-200	330	2.57
M	60	2	25µm Cu	900 X1	2	-200	330	2.57
N	60	2	50µm Cu	80 X1	2	-25	50	2.27
O	60	2	-	900 X1	2	-200	330	2.57
P	30	2	LE1	960 X1	1	-25	50	1.13
Q	30	2	-	700 X1	1	-25	50	1.13
R	30	2	-	1200X1	2	-116	197	2.52
S	30	2	-	1200X1	1	-90	150	2.52
Sagometer settings								
Sag	60	2	-	0.9 X 320	-	84.1	587.4	2.7

## FIGURES

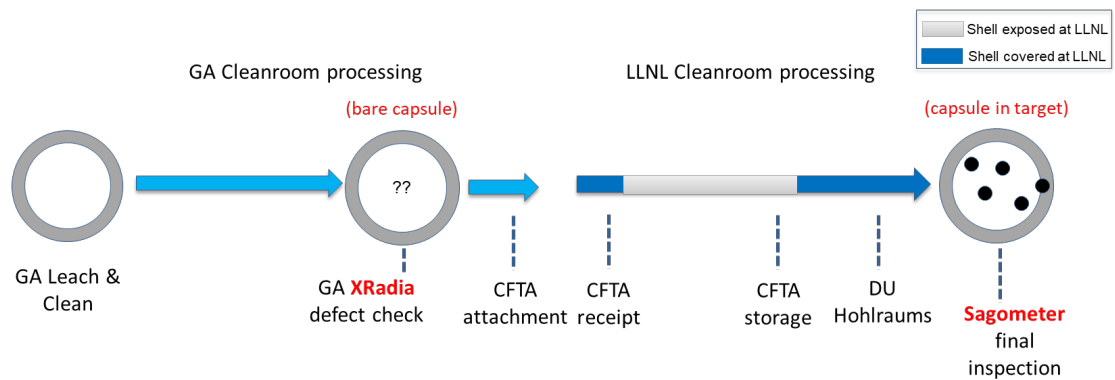


Fig. 1. Summary of HDC capsule lifecycle in terms of processing steps at GA and LLNL.<sup>2</sup>

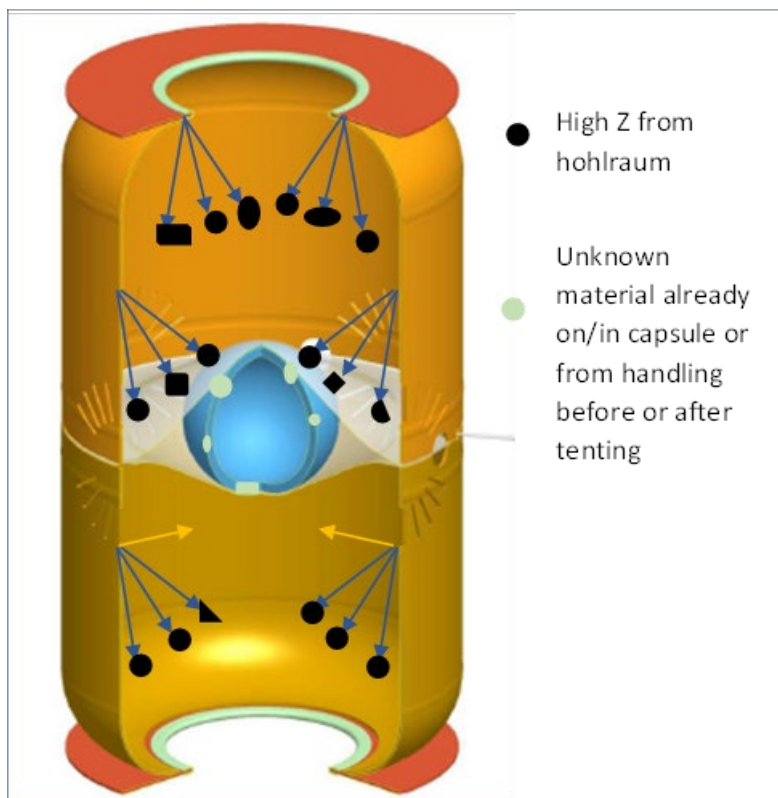


Fig. 2. Possible locations of particles causing Sagometer detections on a typical fusion target. Shown is the HDC capsule suspended by tents inside of a DU or gold hohlraum.<sup>2</sup>

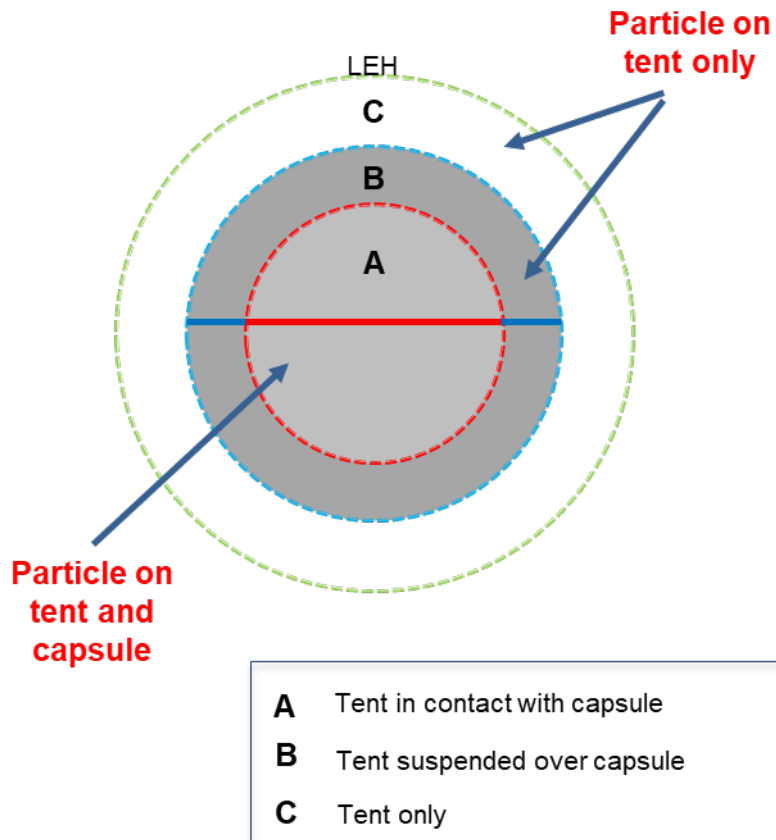


Fig. 3. Projected areas of the capsule and tents as they are seen in Sagometer images.

This view is looking through the top and bottom LEH at the capsule.<sup>2</sup>

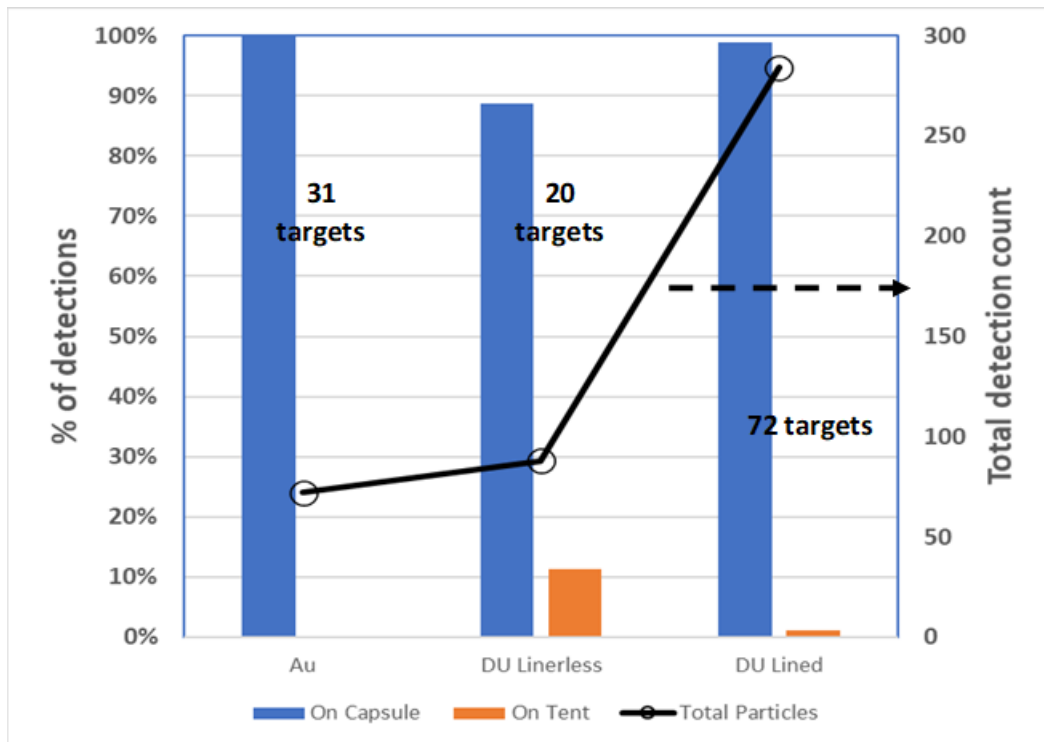


Fig. 4. Review of Sagometer detections on three different hohlraum types, and the location of the detections.<sup>2</sup>

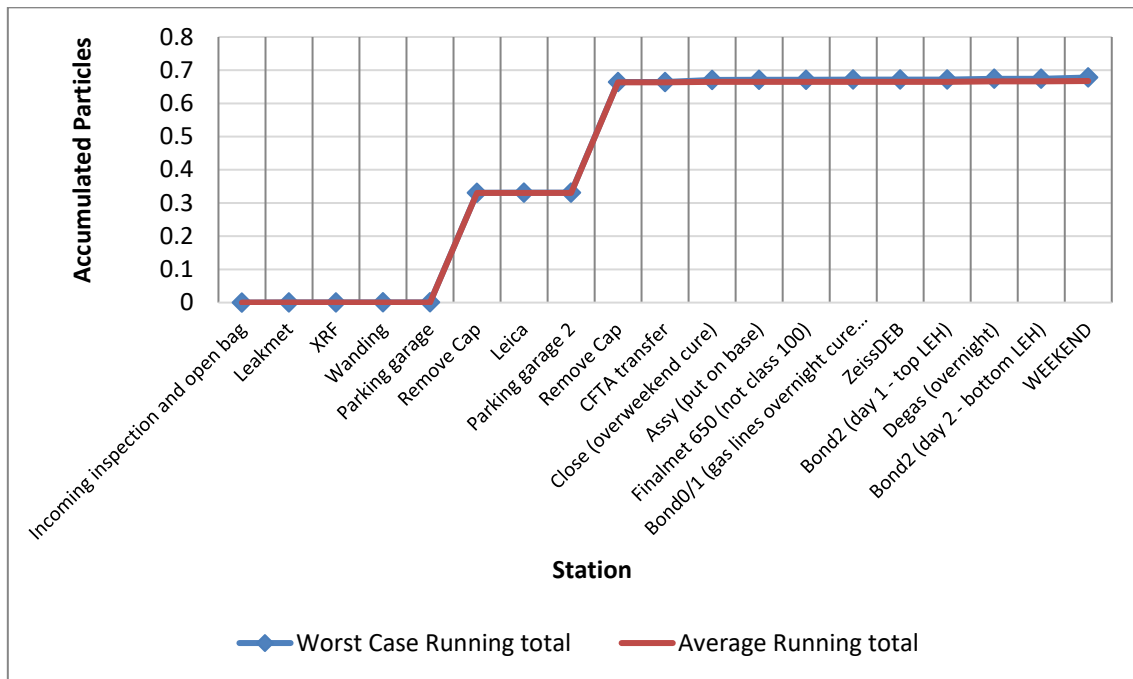


Fig. 5. Worst-case total particles accumulated on the capsule during a standard DT target build at LLNL.<sup>4</sup>

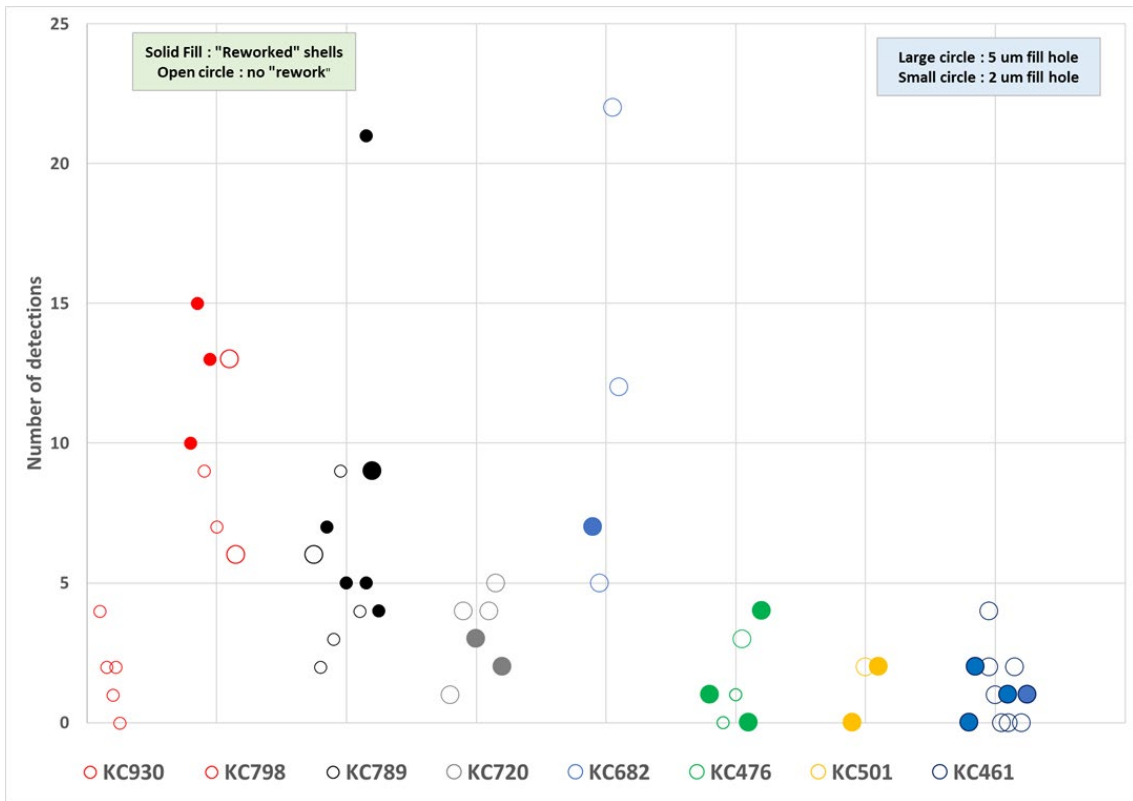


Fig. 6. Capsule detections by manufacturing batch.<sup>2</sup>

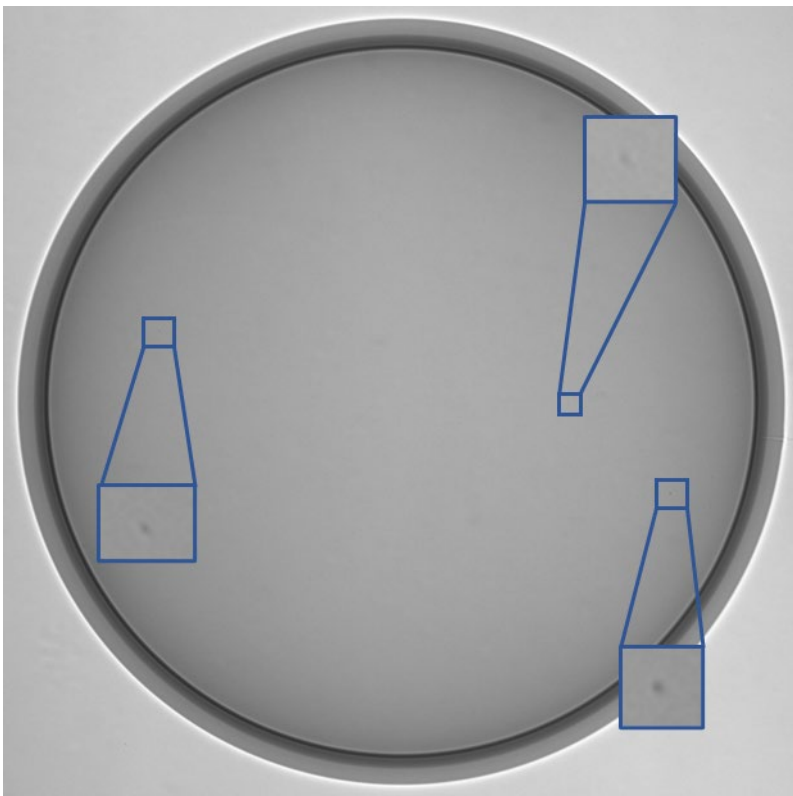


Fig. 7. Sagometer detections on an HDC capsule.

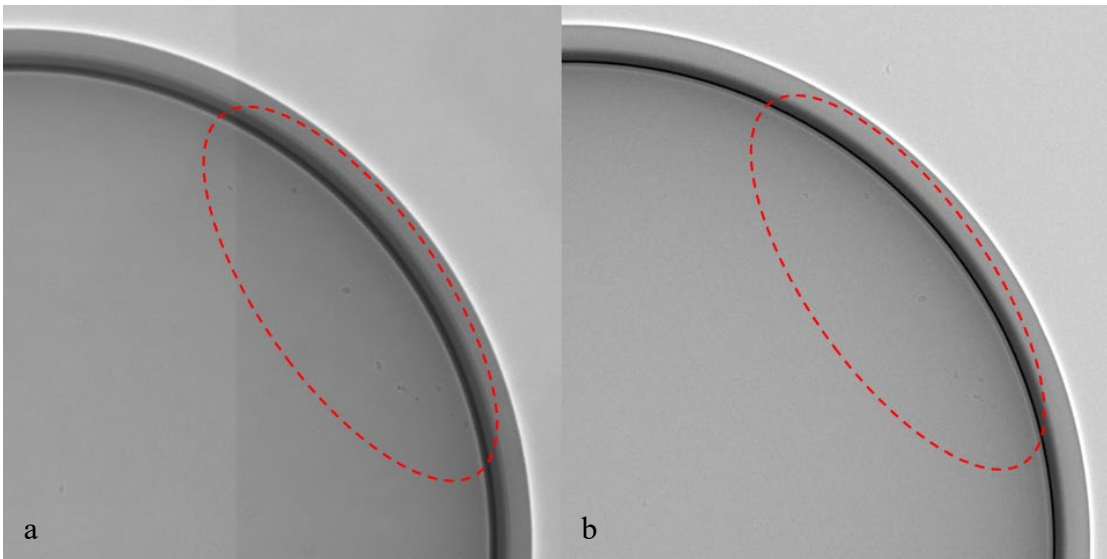


Fig. 8. Sagometer (a) and Xradia (b) radiographs of low Z particles (circled in red) on the same capsule.

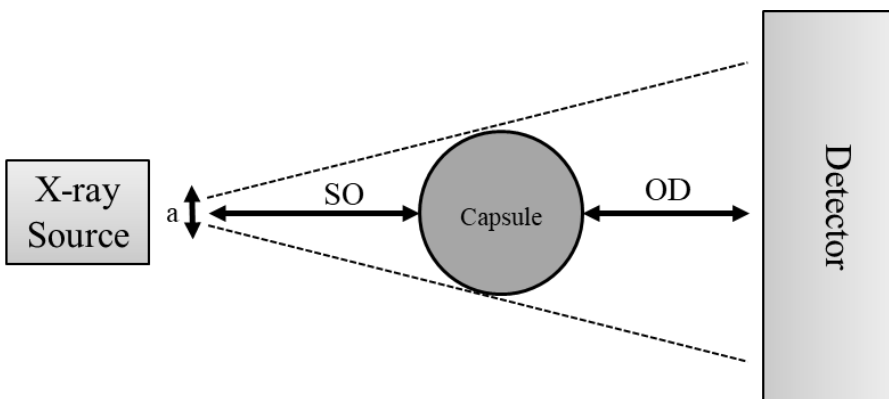


Fig. 9. X-ray imaging geometry for capsule radiography.

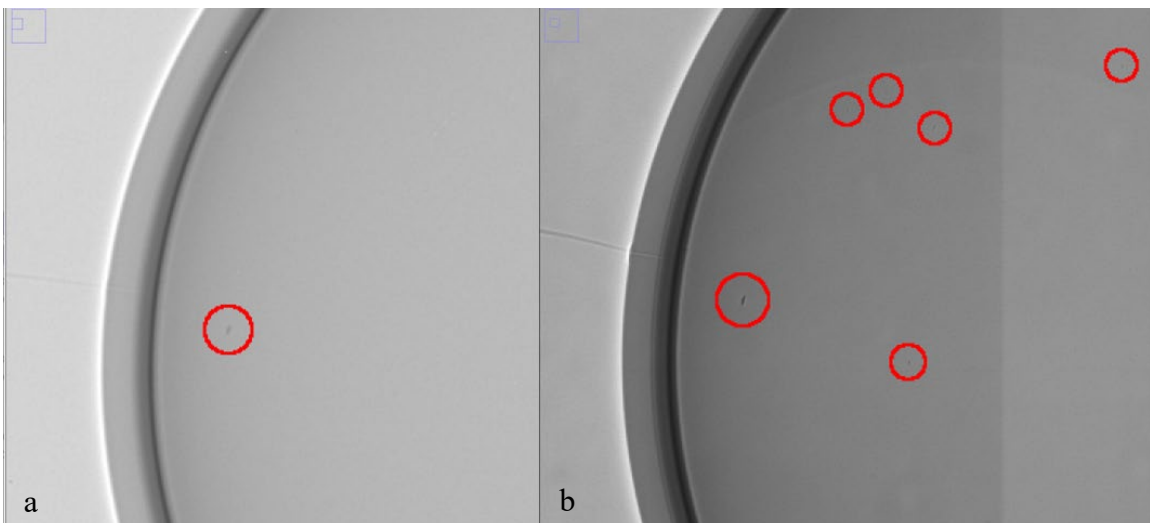


Fig. 10. Xradia image (a) and Sagometer image (b) of the same capsule. Detections identified by the software are circled in red.